ACS OMEGA

http://pubs.acs.org/journal/acsodf

Article

Graphitic Carbon Cloth-Based Hybrid Molecular Catalyst: A Non-conventional, Synthetic Strategy of the Drop Casting Method for a Stable and Bifunctional Electrocatalyst for Enhanced Hydrogen and Oxygen Evolution Reactions

Ram Murthy and Sundaresan Chittor Neelakantan*

Cite This: *ACS Omega* 2022, 7, 32604–32614

Read Online

ACCESS | Metrics & More | Article Recommendations | Supporting Information

ABSTRACT: Hydrogen energy production through water electrolysis is envisaged as one of the most promising, sustainable, and viable alternate sources to cater to the incessant demands of renewable energy storage. Germane to our effort in this field, we report easily synthesizable and very cost-effective isoperthiocyanic acid (IPA) molecular complexes as electrocatalysts for the hydrogen evolution reaction (HER) and oxygen evolution reaction (OER) under acidic and alkaline conditions. The Pd(II)IPA, Co(II)IPA, and Ni(II)IPA complexes were synthesized and were evaluated for HER and OER applications. These complexes when embedded onto graphitized carbon cloth (GrCC) exhibited a significant enhancement in the HER activity in contrast to their pristine counterparts. The hybrid electrocatalyst Pd(II)IPA among the three showed an extremely low overpotential of 94.1 mV to achieve a current density of 10 mA cm^{-2}, while Co(II)IPA and Ni(II)IPA complexes showed overpotentials of 367 and 394 mV, respectively, to achieve a current density of 10 mA cm^{-2}. These complexes on carbon cloth showed decreased charge transfer resistance compared to that of pristine metal complexes. The enhanced catalytic activity of the complexes on carbon cloth can be attributed to the porous and conducting nature of the graphitized carbon cloth. For OER activity, the Pd(II)IPA complex showed an excellent performance with an overpotential value of 210 mV, while Co(II)IPA and Ni(II)IPA exhibited overpotentials of 400 and 270 mV, respectively, to drive a current density of 10 mA cm^{-2} in 0.1 M KOH. This work further widens the scope and application of molecular complexes in combination with an excellent carbon support for renewable energy storage applications.

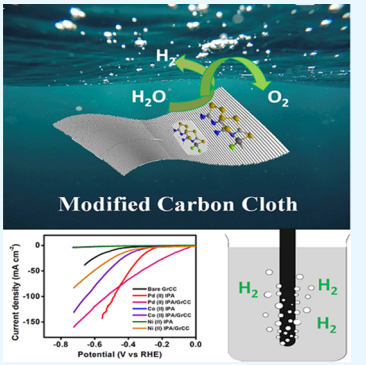

1. INTRODUCTION

The burgeoning demands of fossil fuels and consequential degradation of the environment have raised serious concerns about conventional energy sources. Predominantly, 79.5% of the energy demands are met by the utilization of fossil fuels, which have resulted in an increased carbon footprint, while just 20.5% of the energy requirements are met by renewable energy resources of the global energy consumption.[1] The energy demand is prognosticated to grow to 23 TW in 2030 and is further expected to touch 30 TW in 2050.[2] Since the rate of consumption would far exceed the rate of production of fossil fuels in the near future, scientists and other stakeholders have begun to seriously focus on other alternate and sustainable energy resources that would not only offset the demand but also ensure that there is drastic reduction in the carbon footprint.

As a long-term and sustainable strategy, renewable energy resources such as hydrogen gas which possess clean, efficient, high energy density and environmentally friendly nature are believed to be a potential replacement for fossil fuels with CO_2 emissions. Researchers have been endeavoring to develop fossil fuel-free pathways to produce fuel and chemicals of global importance. This research on the energy sector to reduce fossil fuel dependence can play a major and dominant role in reducing carbon dioxide emission levels in the atmosphere.

The overall water splitting reaction comprises the hydrogen evolution reaction (HER) and oxygen evolution reaction (OER). Platinum[3] based metal electrocatalysts have been used as catalysts for the water splitting reaction due to their optimum binding energy of hydrogen adsorption, Gibbs free energy for atomic hydrogen adsorption (ΔG_H^*), and low activation energy for hydrogen desorption. However, the deterrent with Pt metal is its exorbitant cost, insufficient reserves, and scalability, which hinders the commercialization of Pt-based electrocatalysts.[4] Similarly, Ru[5]- and Ir[6]-based electrocatalysts are considered state-of-the-art catalysts for the oxygen evolution reaction.[7] The high cost, scarcity, and

Received: July 4, 2022
Accepted: August 26, 2022
Published: September 5, 2022

sluggish kinetics of these metals have limited the commercialization of these electrocatalysts.

In this context, non-noble,[8] earth-abundant transition metal[9]-based functional materials as electrocatalysts with a low overpotential and low Tafel slope are believed to be promising for a cleaner economy. A wide range of non-noble metal-based electrocatalysts such as transition metal-based dichalcogenides (1D, 2D), oxides and hydroxides of transition metal, various carbon supports such as carbon nanostructures, nanorods, and polymers, i.e., polyaniline[10] and polypyrrole,[11] are termed as highly efficient HER catalysts with tunable catalytic activity.

To boost the electrocatalytic performance, various carbon supports such as carbon nanotubes[12] (SWCNTs, MWCNT's), fullerenes,[13] graphene,[14] carbon fiber cloth,[15] Ni foam,[16] and porous carbon nanorods are employed owing to their excellent electrochemical stability and conductivity. In recent times, carbon cloth (CC) has gained significant importance due to its textile property giving rise to space and gap, which largely enhance the HER and OER catalytic processes.[17,18] The conventional strategy of drop-casting electrocatalysts on the electrode surface suffers from the problem of leeching. Hence, in the current study, graphitized carbon cloth was chosen as the carbon support to overcome this limitation.

In this work, we demonstrate the synthesis of a transition metal-based coordinate complex involving minimal cost with bifunctional activity for both the HER and OER. The study reports an easy method of integrating isoperthiocyanic acid complexes with graphitized carbon cloth (GrCC) for an enhanced hydrogen evolution reaction and pristine metal complexes for the oxygen evolution reaction under acidic and alkaline conditions (Figure 1).

2. METHODS AND MATERIALS

2.1. Experimentation. Isoperthiocyanic acid was prepared according to the procedure mentioned in the reference.[19]

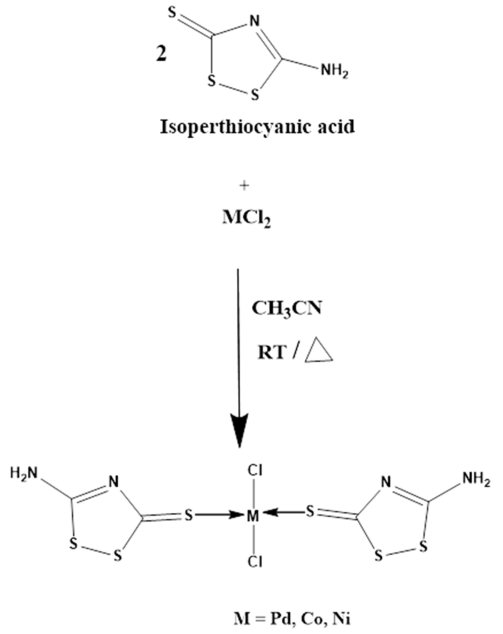

Figure 1. Synthetic protocol for isoperthiocyanic acid metal complexes, $[M(II)(IPA)_2\ Cl_2]$ complex (M = Pd, Co, and Ni).

Metal chloride (1 mmol) and the isoperthiocyanic acid ligand (2 mmol) were stirred in a solvent of anhydrous acetonitrile (60 cm^3) at ambient temperature or heated with gentle reflux. The reflux was continued till there was a change in the color of the solvent mixture. The solid precipitate that formed was filtered, washed with warm acetonitrile, and dried in vacuum.[19]

2.2. Chemicals. The graphitized carbon cloth material was purchased from Sainergy Pvt. Ltd Chennai. Sulfuric acid of 98% and KOH of AR grade were brought from Merck chemicals. Metal salts were procured from Merck chemicals. Milli-Q-grade water was used throughout the experiment. All the solvents and chemicals in the study were used without any further purification.

2.3. Preparation/Modification of Electrodes. A biologic VSP-300 potentiostat electrochemical analyzer and CHI 660E electrochemical workstation were used for electrochemical measurements in a standard three-electrode system. A glassy carbon electrode (GCE) (d = 3 mm)/graphitized carbon cloth (0.5 cm^2) as the working electrode, graphite rod as the counter electrode and saturated calomel electrode, and mercury−mercury oxide alkaline reference electrode were employed as the reference electrode for the HER and OER. The experiments were performed at room temperature, 25 °C. The potentials reported in the study have been recalibrated with respect to the reversible hydrogen electrode (RHE) using the relation $E_{(RHE)} = E + 0.059pH + E_{SCE}$ and oxygen evolution reaction $E_{Hg/HgO} = E + 0.059pH + E_{Hg/HgO}$.

The GCE or rotating disk electrode (RDE) was subjected to a precleaning procedure and was polished with alumina slurry and cleaned. Thereafter, the analyte was drop-cast on the surface of the electrode.

The electrochemical cell was purged with argon gas before the start of the experiment (OER) and nitrogen gas for the HER experiment. The modification of the GCE or RDE was achieved by dispersion of 1.8 mg of analyte in 7:3 ratio of water and isopropanol. Furthermore, Nafion 5% wt solution was added as a binder. A total of 0.2 mg of conducting carbon was added to the dispersion mixture. The resultant dispersion mixture was sonicated for 3 h to obtain a homogeneous ink catalyst. Next, 10 μL of the analyte was drop-cast onto the precleaned glassy carbon surface, and electrochemical measurements were recorded.

3. RESULTS AND DISCUSSION

3.1. FTIR Analysis. Fourier-transform infrared spectroscopy (FTIR) spectra of M(II) IPA complexes were recorded within the range of 4000−450 cm^{-1} to understand the coordination mode of the isoperthiocyanic acid ligand with the metal atom. It was observed that all of the functional group peaks did not show a significant shift in the frequency of the coordination mode with the metal. The complexes showed asymmetric and symmetric (ν-N-H) modes of the $-NH_2$ group, which occur at 3240 and 3210 cm^{-1}, respectively. The intense band at 1310 cm^{-1} is assigned to the (ν-C-N) vibration. The peaks at 1510 and 627 cm^{-1} can be ascribed to the (ν-C═N) group and (ν-NH_2) wag, respectively. All the three complexes showed a band at the 995−1000 cm^{-1} characteristic peak of the (ν-C═S) exocyclic thiocarbonyl group. The exocyclic sulfur group (ν-C═S) of the ligand showed a band at 995 cm^{-1}, which marginally shifted to 1000 cm^{-1} upon complexation. This indicated that the isoperthio-

https://doi.org/10.1021/acsomega.2c04199
ACS Omega 2022, 7, 32604−32614

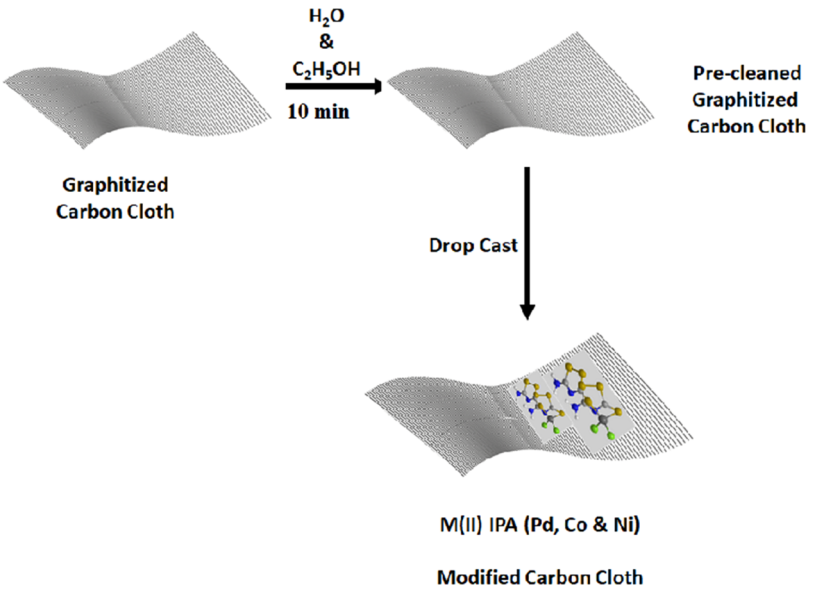

Figure 2. Schematic representation of immobilization of molecular complexes on graphitized carbon cloth by the drop casting method under room temperature conditions.

cyanic acid ligand is bound to the metal ion through the exocyclic sulfur group (ν-C═S).[19]

^{1}H NMR spectra of the complexes were recorded and are described in detail in Supporting Information Section S2. In the case of Pd(II)IPA, Co(II)IPA, and Ni(II)IPA complexes, amine peaks were observed at δ 9.79 and δ 9.73 corresponding to amine protons. Furthermore, ^{13}C NMR spectra of isoperthiocyanic acid complexes were recorded. Pd(II)IPA, Co(II)IPA, and Ni(II)IPA exhibited thiocarbonyl and amine peaks at δ 209.1 and 184.01, respectively.

The UV−vis spectra were obtained; the complexes did not show any change in the wavelength band compared to that of the isoperthiocyanic acid ligand. UV−vis spectral data failed to confirm the possible coordination mode of isoperthiocyanic acid with the metal atom. Edwards et al. studied the isoperthiocyanic acid complexes and revealed that only X-ray photoelectron spectroscopy (XPS) analysis confirms the complex formation and coordination mode of the isoperthiocyanic acid ligand with the metal atom.[19]

3.2. Thermogravimetric Analysis (TGA). TGA analysis was performed for the complexes of IPA as shown in Figure 4a given below. In the case of Pd(II), Co(II), and Ni(II) complexes of IPA, an initial weight loss of 10% is attributed to the loss of chloride ions in the form of hydrochloric acid. Subsequently, in the temperature range of 200−600 °C, the decomposition of the isoperthiocyanic acid ligand is observed, which accounts for the majority of weight loss of 80%. In addition, at temperatures of 800−1000 °C, the metal oxide remained as the final product with a weight loss of 10% and remained constant at increasing temperatures (Figure 4a).

3.3. Scanning Electron Microscopy (SEM). Scanning electron microscopy was performed to understand the morphology of the complexes. SEM images were recorded at a magnification scale of 2 μm, and Pd(II)IPA and Ni(II)IPA complexes were found to possess a flaky morphology. The Co(II)IPA complex was found to exhibit a rod-like crystalline morphology. From Figure 3a−d, the complexes were found to possess an increased space and cavity in comparison to the ligand.

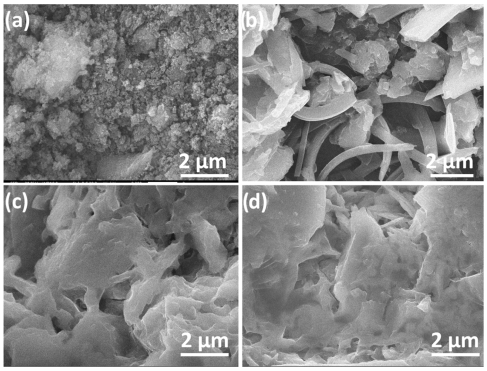

Figure 3. Scanning electron microscopy images of the isoperthiocyanic acid ligand and its complexes. (a) Pd(II) IPA, (b) Co(II) IPA, (c) Ni(II) IPA, and (d) isoperthiocyanic acid (IPA) ligand.

3.4. Vibrating Sample Magnetometer (VSM). M(II)-IPA complexes were subjected to magnetic study through VSM analysis to assess the magnetic properties of the Pd(II), Co(II), and Ni(II) complexes of the IPA ligand. As evidenced in Figure 4b, Pd(II) and Co(II) complexes exhibit diamagnetism where the unpaired electrons are involved in bonding. On the contrary, the Ni(II) IPA complex displays ferromagnetic behavior (Figure 4b).

3.5. X-ray Photoelectron Spectroscopy (XPS). X-ray photoelectron spectroscopy was performed to understand the coordination mode of the ligand. The binding energies of C 1s and N 1s of the free ligand were not affected upon coordination with the metal atom. The chemical shift difference between two sulfur sites decreases from 2.1 to 1.3 eV on coordination (Figure 5). The binding energies of S, 2p, the endocyclic sulfur atoms, did not show any change after coordination with the metal atom. However, the relative binding energy of the exocyclic thione sulfur shifts by +(0.6−0.9 eV). From the literature, it is observed that thiourea complexes show a shift in the binding energy by ca. +0.8 eV upon coordination with the metal atom. Hence, XPS spectra confirmed the chelation of isoperthiocyanic acid through the

https://doi.org/10.1021/acsomega.2c04199
ACS Omega 2022, 7, 32604−32614

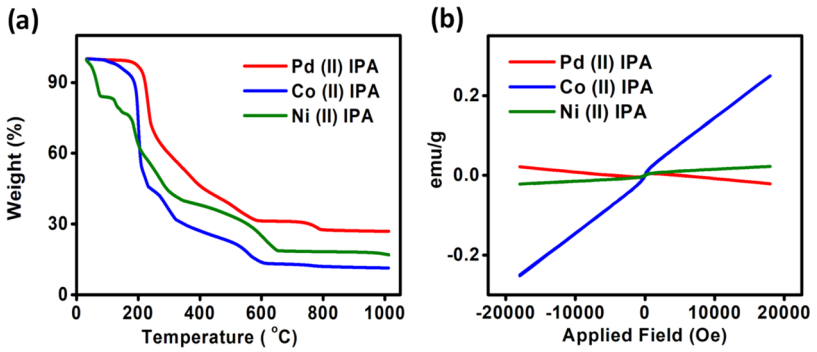

Figure 4. (a) Thermogravimetric analysis graph of isoperthiocyanic acid complexes and (b) vibrating sample magnetometer plot (VSM) of M(II) IPA complexes depicting the magnetic nature of the complexes.

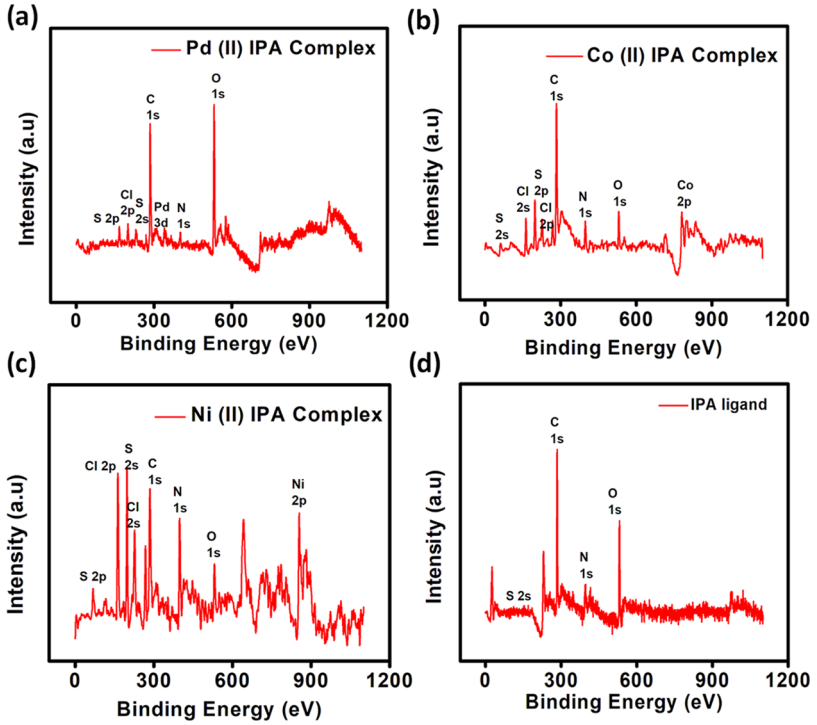

Figure 5. XPS spectra of isoperthiocyanic acid and its complexes. (a) Pd(II) IPA, (b) Co(II) IPA, (c) Ni(II) IPA complex, and (d) isoperthiocyanic acid ligand.

exocyclic sulfur atom with the respective metal ions (Figure 5).[19]

To confirm the successful immobilization of molecular complexes on graphitized carbon cloth, XPS analysis was performed for complexes on GrCC. From Figure 6a,b given below, it is evident that GrCC shows a characteristic peak at 337.8 and 342.1 eV corresponding to Pd $3d_{3/2}$ and Pd $3d_{5/2}$, respectively[20,21] before the linear sweep voltammetry (LSV) stability test (Figure 6e). The spectra show the presence of the N 1s peak with a binding energy value of 400.1 eV (Figure 6i) and sp^2-hybridized C 1s peak at 284.5 eV (Figure 6h). In the case of Pd(II)IPA on GrCC after a 6 h stability test, it was observed that no trace of the Pd metal ion was found on graphitized carbon cloth. Furthermore, Ni(II)IPA on GrCC showed the characteristic Ni 2p metal ion peak at 853.2 eV, and other peaks remain constant (Figure 6c,g).[22,23]

3.6. Hydrogen Evolution Reaction. The HER electrocatalytic activity of the three isoperthiocyanic acid (IPA) complexes (M = Pd, Co, and Ni) was investigated in 0.5 M H_2SO_4 (pH = 0). The catalyst mass loading of 0.282 mg cm^{-2} was achieved on the GCE electrode surface. Results are shown in Figure 7, showcasing the excellent catalytic activity evidenced by the onset potential and overpotential values. The linear sweep voltammetry curves were recorded in the pristine form and hybrid form for all the three complexes. The pristine Pd(II) IPA complex showed maximum activity with an overpotential of 276 mV (vs RHE) to drive a geometrical current density of 10 mA cm^{-2} and overall current density of 147 mA cm^{-2} at an overpotential of 890 mV. The Ni(II) and Co(II) IPA pristine complexes produce a cumulative 4 mA cm^{-2} current density, shown in Figure 7a. Hence, carbon cloth was used as a support to enhance the catalytic activity of the complexes.

To improve the HER performance of the catalyst, the electrocatalyst was directly immobilized on the graphitized carbon cloth material by the drop casting method and dried thoroughly (Figure 2). A catalyst mass loading of 0.04 mg cm^{-2} was attained on the GrCC. Before that, GrCC was

https://doi.org/10.1021/acsomega.2c04199
ACS Omega 2022, 7, 32604−32614

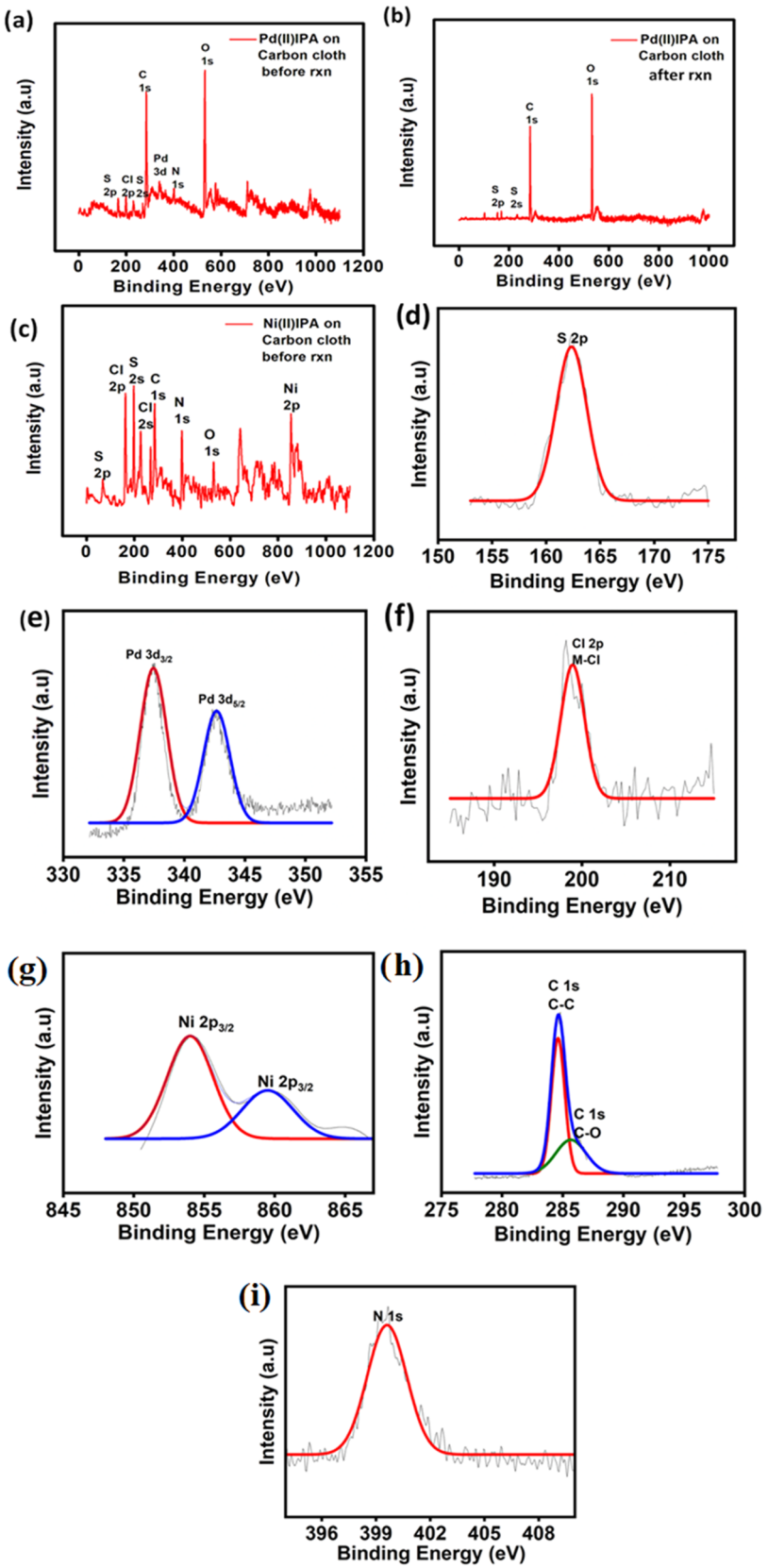

Figure 6. XPS spectra of isoperthiocyanic acid complexes on carbon cloth before the linear sweep voltammetry test (a) Pd(II)IPA on carbon cloth before the reaction, (b) Pd(II)IPA on carbon cloth after the reaction, and (c) Ni(II)IPA on carbon cloth before the reaction. (d) XPS peak of S 2p on GRCC. (e) XPS peak of Pd $3d_{3/2}$ and Pd $3d_{5/2}$ of Pd(II)IPA/GrCC on GrCC. (f) XPS peak of Cl 2p on GRCC. (g) XPS peak of Ni $2p_{3/2}$ of Ni(II)IPA/GrCC on GrCC. (h) XPS peak of C 1s on GrCC. (i) XPS peak of N 1s on GrCC.

https://doi.org/10.1021/acsomega.2c04199
ACS Omega 2022, 7, 32604−32614

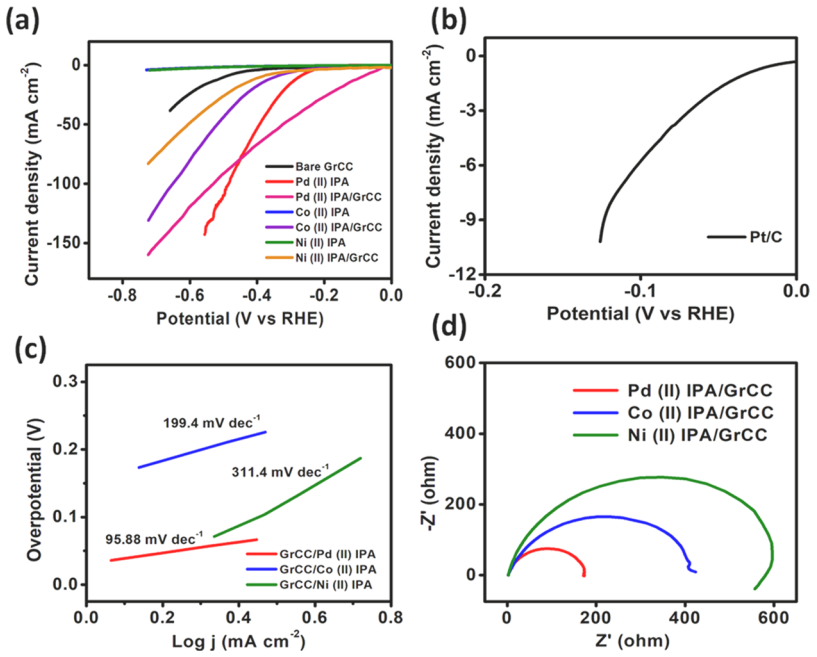

Figure 7. (a) Linear sweep voltammetry (LSV) curves of pristine M(II) IPA and M(II) IPA/GrCC complexes in 0.5 M H_2SO_4. (b) LSV plot of 10% Pt/C in 0.5 M H_2SO_4. (c) Corresponding Tafel slopes of linear polarization curves of M(II) IPA/GrCC under acidic conditions. (d) Nyquist plot of M(II) IPA/GrCC hybrid complexes in 0.5 M H_2SO_4.

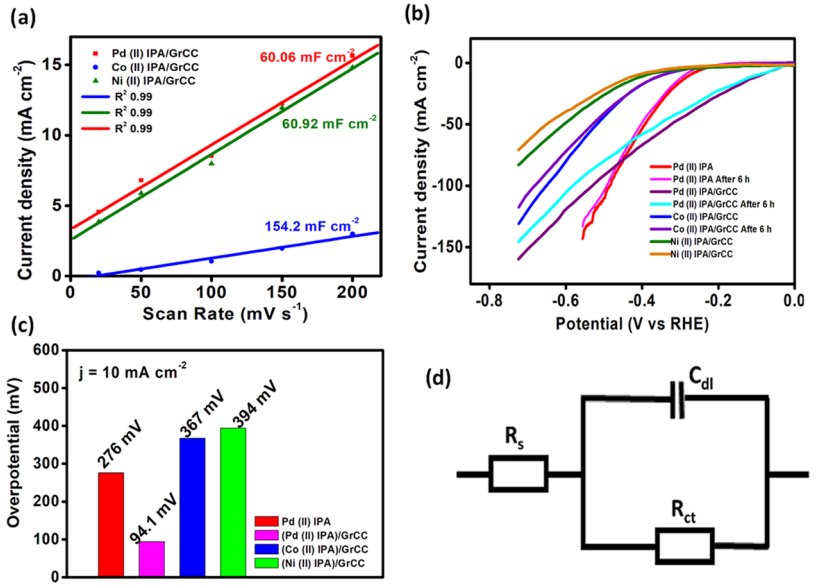

Figure 8. (a) Capacitance double-layer (C_{dl}) evaluation of M(II) IPA/GrCC complexes in 0.5 M H_2SO_4. (b) Stability study through LSV curves for a period of 6 h in acid electrolyte. (c) Plot of the overpotential of the pristine and hybrid complexes to achieve 10 mA cm^{-2}. (d) Equivalent circuit used for fitting Nyquist plots.

sequentially sonicated in ethanol and water for 10 min each. The Pd(II), Co(II), and Ni(II) complexes of IPA on carbon cloth exhibited enhanced catalytic activity, and the overpotential of the electrocatalyst lowered significantly. The three complexes, Pd(II), Co(II), and Ni(II), on the graphitized carbon cloth showed an overpotential of 94.1, 367, and 394 mV to drive a geometric current density of 10 mA cm^{-2} (Figure 8c) and a cumulative current density of 158, 130, and 90 mA cm^{-2}, respectively (Figure 7b). The presence of the graphitized carbon cloth enhanced the catalytic activity owing to its porous and conducting property of the carbon cloth. The synergistic interaction between GrCC and carbon cloth boosted the catalytic performance of the M(II)IPA complexes.

The kinetics of the HER mechanism was investigated using Tafel slope studies, and Log j vs overpotential (η) was plotted using the relation $\eta = a \pm b \log j$. The Tafel slopes of the three hybrid electrocatalysts were determined. Tafel slopes of 95.88, 199.4, and 311.4 mV dec^{-1} were obtained for the complexes Pd(II), Co(II), and Ni(II) IPA immobilized on GrCC, respectively, depicted in Figure 7c.

The impedance analysis of the complexes inside the electrochemical cell was done by electrochemical impedance spectroscopy (EIS) within the frequency range of 200 kHz to

https://doi.org/10.1021/acsomega.2c04199
ACS Omega 2022, 7, 32604−32614

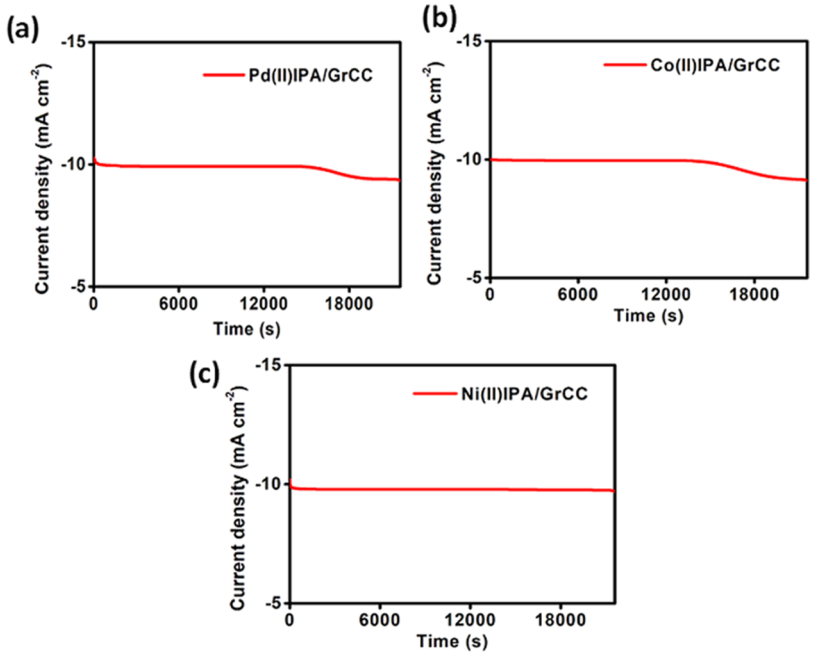

Figure 9. Durability test performed for M(II)IPA using the chronoamperometry technique at the constant potential in 0.5 M H_2SO_4. (a) Pd(II)BTT/GrCC, −0.094 V, (b) Co(II)IPA/GrCC, −0.367 V, and (c) Ni(II)IPA, −0.394 V.

Table 1. Comparison of the HER Catalytic Activities of M(II) IPA Complexes with Those of the Existing Transition Metal-Based Electrocatalyst

si. no	electrocatalyst	electrolyte	overpotential (mV)	Tafel slope (mV dec^{-1})	reference
1.	$NiSe_2$@NG	0.5 M H_2SO_4	248	74.2	26
2.	Mo_2C-GNR's	0.5 M H_2SO_4	167	74	27
3.	CoS_x@MoS_2	0.5 M H_2SO_4	239	103	28
4.	Ni@CNT's	0.5 M H_2SO_4	261	88	29
5.	Pd@TiO_2-H	0.5 M H_2SO_4	430	63	30
6.	$PdMoS_2$	0.5 M H_2SO_4	137	70	31
7.	Pd(II) IPA/GrCC	0.5 M H_2SO_4	94.1	95.88	current work

0.1 Hz with a signal amplitude perturbation of 10 mV s^{-1}. The Pd(II) IPA complex showed the least charge transfer resistance of 190 ohms in comparison to that of the Co(II) and Ni(II) complexes of 410 and 580 ohms, respectively, reflected in Figure 7d. The catalytic performance was much higher vis-a-vis the bare graphitized carbon cloth and modified GCE electrode results. The impedance analysis further proved that the carbon cloth support aids in the facile electron flow at the electrode (GrCC)/electrolyte interface.

The high catalytic activity of the hybrid electrocatalysts, Pd, Co, and Ni complexes, of IPA was investigated through the determination of the double-layer capacitance. Cyclic voltammetric study at different scan rates, ranging from 20 to 200 mV was performed. The plot of Δj ($j_a - j_c$) against the scan rate yielded the slope value (C_{dl}). From Figure 8a, it is observed that the hybrid electrocatalysts showed a C_{dl} value of 60.06, 154.2, and 60.92 mF cm^{-2} respectively. The electrochemical activity is well interpreted through the electrochemical active surface area (ESCA), which is directly proportional to the double-layer capacitance.[24] The linear plot (Figure 8a) revealed that the electrocatalytic process is a diffusion-controlled process. The current is due to the facile electron flow at the electrode/electrolyte interface.

$$C_{dl} = \frac{\Delta j}{V} \quad (1)$$

$$\text{ECSA} = \frac{C_{dl}}{C_s} \quad (2)$$

where Δj is the current density (mA cm^{-2}), V is the potential, and C_s is the standard specific capacitance (C_s −0.04 mF cm^{-2}).[25] Pd(II)IPA/GrCC, Co(II)IPA/GrCC, and Ni(II)-IPA/GrCC hybrid complexes involve ECSA values of 0.15, 0.385, and 0.152 m^2 g^{-1}, respectively. The high surface area of the electrocatalysts is due to the presence of the porous and weaved textile framework of the carbon cloth. The mass activity of the three hybrid electrocatalysts was determined from current density per unit mass of M(II)IPA/GrCC electrocatalysts. The mass activity of the hybrid electrocatalysts Pd(II)IPA/GrCC, Co(II)IPA/GrCC, and Ni(II)IPA/GrCC was found to be 3.675, 3.25, and 2.25 A mg^{-1}, respectively.

The stability study of the electrocatalysts was performed for 6 h from the linear sweep voltammogram technique. It was found that all three M(II)IPA complexes exhibited 85% current density retention from the initial cycle of the experiment. Figure 8b depicts the stability of the three electrocatalysts in 0.5 M H_2SO_4. The durability test was performed using the chronoamperometric technique at a constant potential, as depicted in Figure 9a−c. It is evident that

https://doi.org/10.1021/acsomega.2c04199
ACS Omega 2022, 7, 32604−32614

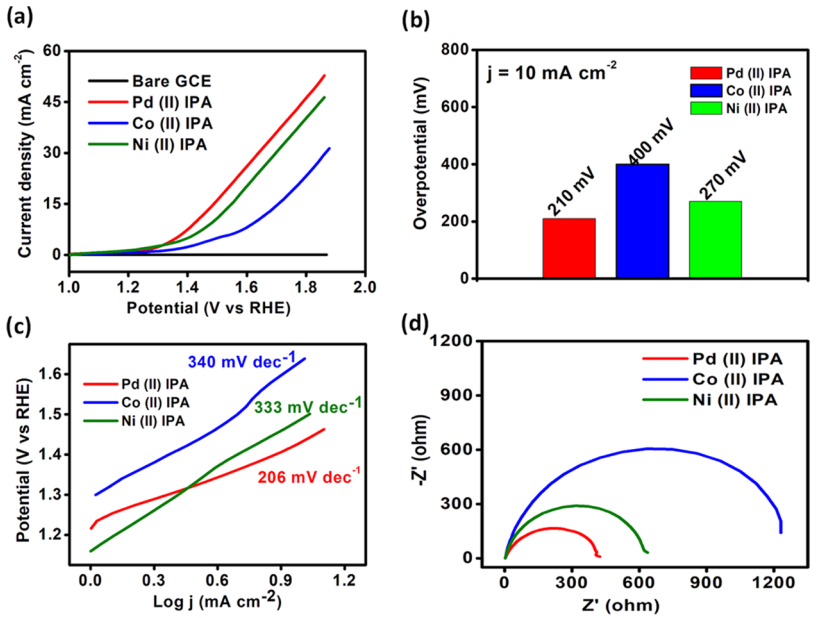

Figure 10. (a) Linear sweep voltammetry (LSV) plots of pristine M(II) IPA complexes in 0.1 M KOH. (b) Plot of the overpotential depicting the potential required to produce 10 mA cm^{-2} current density in 0.1 M KOH. (c) Tafel plot derived from the linear sweep voltammetry data of M(II) IPA in 0.1 M KOH. (d) Nyquist plot of M(II) IPA and M(II) IPA/GrCC complexes under alkaline conditions.

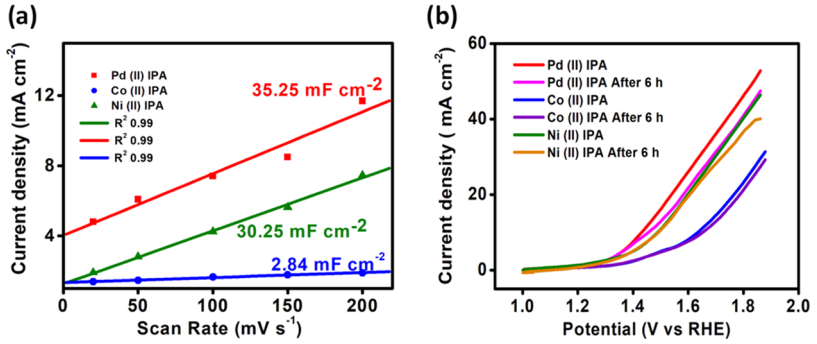

Figure 11. (a) Capacitance double-layer (C_{dl}) evaluation of M(II) IPA/GrCC complexes in 0.1 M KOH solution. (b) Stability study through linear sweep voltammetry studies for a period of 6 h in 0.1 M KOH.

the molecular complexes exhibit stable performance for 4h after which the current density was found to wane gradually. Though, molecular complexes possess inherent durability limitation, they can be augmented with better carbon supports (Table 1).

3.7. Oxygen Evolution Reaction. The OER performance of M(II) IPA (M = Pd, Co, and Ni) complexes was investigated in 0.1 M KOH in an oxygen-saturated system. A rotating disk electrode setup at 1600 rpm was used to perform linear sweep voltammetry (LSV). The electrochemical setup involved a RDE as the working electrode, graphite rod as the auxiliary electrode, and mercury−mercury oxide as the reference electrode.

LSV curves were recorded within the range of 0−1 V with a scan rate of 50 mV s^{-1} in 0.1 M KOH, as depicted in Figure 10a. The potentials reported have been normalized with respect to a reversible hydrogen electrode (RHE). The oxidation peak of the Ni(II) IPA complex lies between 1.35 and 1.45 V (vs RHE) corresponding to the formation of the NiOOH intermediate in the mechanism. The Ni(II) IPA complex required an overpotential of 270 mV (vs RHE) to achieve a current density of 10 mA cm^{-2}. Furthermore, Pd(II) and Co(II) complexes of IPA exhibited a current density of 10 mA cm^{-2} at an overpotential of 210 and 400 mV (vs RHE), respectively (Figure 10b).

Pd(II) IPA produced a cumulative current density of 57.12 mA cm^{-2} at 1.897 V, and Ni(II) and Co(II) exhibited an overall current density of 43.13 and 32.83 mA cm^{-2} at 1.863 V, respectively (Figure 10a).

The Tafel slope is one of the important parameters to investigate the kinetics of the OER reaction. Tafel equation $\eta = a + b \log j$ (η = overpotential, j = current density, and b = Tafel slope). From Figure 10c, it is observed that Pd(II) IPA and Ni(II) IPA exhibited Tafel slope values of 206 mV dec^{-1} and 333 mV dec^{-1}, respectively, whereas Co(II) IPA showed a value of 340 mV dec^{-1}. Pd and Ni complexes of IPA possess favorable kinetics toward OER activity. Stability tests were carried out to understand the durability standard of the electrocatalyst for 6 h using the LSV technique. Chronoamperometry was performed to evaluate the durability of the electrocatalysts. The complexes showed stable current density of 10 mA cm^{-2} for 4h after which current density decreased gradually Figure 12. The current density decreased gradually

https://doi.org/10.1021/acsomega.2c04199
ACS Omega 2022, 7, 32604−32614

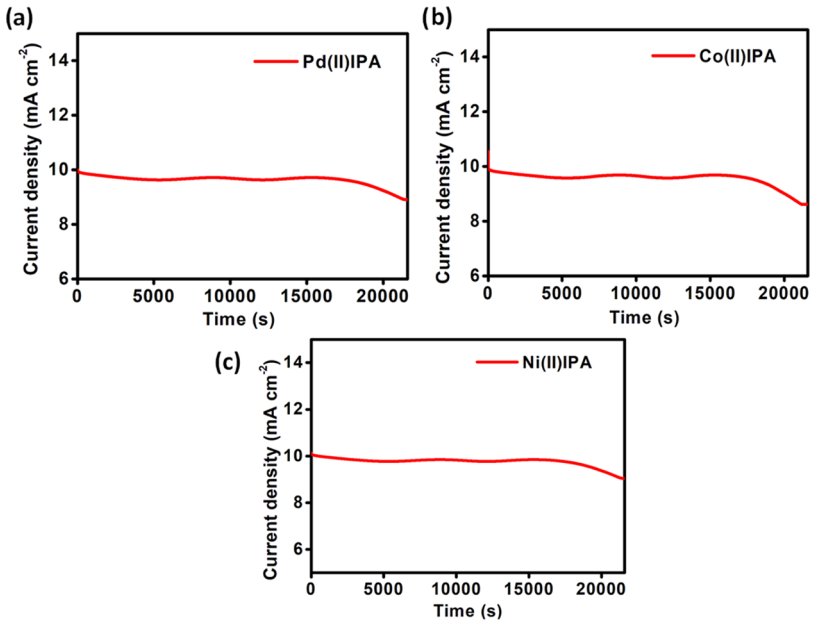

Figure 12. Durability test performed for M(II)IPA complexes by chronoamperometry in 0.1 M KOH at constant potential. (a) Pd(II)IPA, (b) Co(II)IPA, and (c) Ni(II)IPA.

with a retention of 85% of the current density from the initial experiment, Figure 11b.

Impedance analysis was performed for all the three metal complexes under alkaline conditions, shown in Figure 10d; the Pd complex of isoperthiocyanic showed the least charge transfer resistance (R_{ct}) of 400 ohms, implying favorable OER kinetics compared to that of Ni(II) and Co(II) complexes of isoperthiocyanic acid, which showed an R_{ct} value of 620 and 1200 ohms, respectively .

The capacitance double-layer values of M(II)IPA complexes were found to be 35.25, 2.84, and 30.25 mF cm^{-2}. ECSA values were found to be 0.088, 0.0071, and 0.0756 $m^2\ g^{-1}$. The large space availability in the complexes has led to a large electrochemical active surface area. The mass activity of the three electrocatalysts was determined from current density per unit mass loading. The Pd(II), Co(II), and Ni(II) IPA complexes showed a mass activity of 0.202, 0.154, and 0.116 A mg^{-1}, respectively (Table 2).

4. CONCLUSIONS

The isoperthiocyanic acid complexes (M = Pd, Co, Ni) were synthesized and characterized using various techniques. The Pd(II)IPA complex on the graphitized carbon cloth was employed as a working electrode for the hydrogen evolution reaction. The complexes act as bifunctional electrocatalysts under both acidic and alkaline conditions. The Pd(II)IPA complex on graphitized carbon cloth exhibited an extremely low overpotential of 94.1 mV to achieve a current density of 10 mA cm^{-2} compared to the pristine Pd(II)IPA complex with an overpotential of 276 mV to drive a current density of 10 mA cm^{-2} in 0.5 M H_2SO_4. The hybrid electrocatalyst M(II)IPA/GrCC enhances the catalytic performance by exposing more active sites and synergistic charge transfer. The enhanced electrocatalytic activity is due to the porous and conducting nature of carbon cloth.

For the OER, it was found that sulfur serves as the active site for binding of protons, and due to increased oxygen evolution, it was found that sulfur possesses optimum binding energy, endowing the electrocatalyst with high intrinsic catalytic activity toward the OER. The pristine Pd(II)IPA complex showed a low overpotential of 210 mV to achieve a current density of 10 mA cm^{-2}. This work culminated in developing low-cost, highly efficient transition metal complexes, which were investigated as efficient electrocatalysts for HER and OER applications.

Table 2. Comparison of the OER Activities of M(II) IPA with Those of the Existing Transition Metal-Based Electrocatalyst in 0.1 M KOH

si. no	electrocatalyst	overpotential (mV vs RHE)	Tafel slope (mV dec^{-1})	reference
1.	3D $NiCoSe_2$/NF	183	88	32
2.	$NiO/NiCo_2O_4$	430	49	33
3.	NiFeB-P MNs	252	35.2	34
4.	PdONPs@ Co_3O_4	250	58	35
5.	hierarchical Pd	196	51.3	36
6.	PdP_2@CB	270	78.6	37
7.	Pd(II) IPA	210	206	current work

■ ASSOCIATED CONTENT

Supporting Information

The Supporting Information is available free of charge at https://pubs.acs.org/doi/10.1021/acsomega.2c04199.

Characterization and proposed mechanism for the hydrogen evolution reaction (PDF)

■ AUTHOR INFORMATION

Corresponding Author

Sundaresan Chittor Neelakantan − *Department of Chemistry, Sri Sathya Sai Institute of Higher Learning, Bengaluru 560067, India;* orcid.org/0000-0001-7327-684X; Email: cnsundaresan@sssihl.edu.in

https://doi.org/10.1021/acsomega.2c04199
ACS Omega 2022, 7, 32604−32614

Author

Ram Murthy − *Department of Chemistry, Sri Sathya Sai Institute of Higher Learning, Bengaluru 560067, India;* orcid.org/0000-0003-1236-1500

Complete contact information is available at: https://pubs.acs.org/10.1021/acsomega.2c04199

Notes

The authors declare no competing financial interest.

■ ACKNOWLEDGMENTS

The authors express their deep sense of gratitude to their founder Chancellor Bhagavan Sri Sathya Sai Baba for being a constant source of inspiration and motivation for the work. R.M. is grateful to Dr. B V V S Pavan Kumar, IIT Roorkee, for the XPS characterization facility. R.M. is thankful to both Prof. Noriyoshi Matsumi and Dr. Rajashekar Badam from the Japan Advanced Institute of Science and Technology (JAIST) for hands-on experience on various instruments during the "Sakura Science Program". The authors thank Dr. Raman Vedarajan from the ARCI for insightful discussions. R.M. is thankful to M. Bhargava Sai for his valuable inputs for the graphical abstract. The authors acknowledge the Central Research Instrumentation Facility (CRIF) for the characterization facility. The authors thank SSSIHL for financial support for carrying out this work.

■ REFERENCES

(1) Zhu, J.; Hu, L.; Zhao, P.; Lee, L. Y. S.; Wong, K.-Y. Recent Advances in Electrocatalytic Hydrogen Evolution Using Nanoparticles. *Chem. Rev.* **2020**, *120*, 851−918.

(2) Lewis, N. S.; Nocera, D. G. Powering the planet: Chemical challenges in solar energy utilization. *Proc. Natl. Acad. Sci. U.S.A.* **2006**, *103*, 15729−15735.

(3) Yu, J.; Du, X.; Liu, H.; Qiu, C.; Yu, R.; Li, S.; Ren, J.; Yang, S. Mini Review on Active Sites in Ce-Based Electrocatalysts for Alkaline Water Splitting. *Energy Fuels* **2021**, *35*, 19000−19011.

(4) Li, C.; Baek, J.-B. Recent Advances in Noble Metal (Pt, Ru, and Ir)-Based Electrocatalysts for Efficient Hydrogen Evolution Reaction. *ACS Omega* **2020**, *5*, 31−40.

(5) Wang, G.; Chen, X.; Liu, S.; Wong, C.; Chu, S. Mechanical Chameleon through Dynamic Real-Time Plasmonic Tuning. *ACS Nano* **2016**, *10*, 1788−1794.

(6) Yuan, C.-Z.; Hui, K. S.; Yin, H.; Zhu, S.; Zhang, J.; Wu, X.-L.; Hong, X.; Zhou, W.; Fan, X.; Bin, F.; Chen, F.; Hui, K. N. Regulating Intrinsic Electronic Structures of Transition-Metal-Based Catalysts and the Potential Applications for Electrocatalytic Water Splitting. *ACS Mater. Lett.* **2021**, *3*, 752−780.

(7) Aoudj, S.; Khelifa, A.; Drouiche, N.; Belkada, R.; Miroud, D. Simultaneous removal of chromium(VI) and fluoride by electrocoagulation−electroflotation: Application of a hybrid Fe-Al anode. *Chem. Eng. J.* **2015**, *267*, 153−162.

(8) Zhang, L.; Cao, X.; Feng, C.; Zhang, W.; Wang, Z.; Feng, S.; Huang, Z.; Lu, X.; Dai, F. Interfacial Mo−N−C Bond Endowed Hydrogen Evolution Reaction on MoSe2@N-Doped Carbon Hollow Nanoflowers. *Inorg. Chem.* **2021**, *60*, 12377−12385.

(9) Chung, D. Y.; Jun, S. W.; Yoon, G.; Kim, H.; Yoo, J. M.; Lee, K.-S.; Kim, T.; Shin, H.; Sinha, A. K.; Kwon, S. G.; Kang, K.; Hyeon, T.; Sung, Y.-E. Large-Scale Synthesis of Carbon-Shell-Coated FeP Nanoparticles for Robust Hydrogen Evolution Reaction Electrocatalyst. *J. Am. Chem. Soc.* **2017**, *139*, 6669−6674.

(10) Huang, M.; Zhang, H.; Yin, S.; Zhang, X.; Wang, J. PtAg Alloy Nanoparticles Embedded in Polyaniline as Electrocatalysts for Formate Oxidation and Hydrogen Evolution. *ACS Appl. Nano Mater.* **2020**, *3*, 3760−3766.

(11) Lattach, Y.; Fortage, J.; Deronzier, A.; Moutet, J.-C. Polypyrrole-Ru(2,2′-bipyridine)32+/MoSx Structured Composite Film As a Photocathode for the Hydrogen Evolution Reaction. *ACS Appl. Mater. Interfaces* **2015**, *7*, 4476−4480.

(12) Huang, B.; Chen, L.; Wang, Y.; Ouyang, L.; Ye, J. Paragenesis of Palladium−Cobalt Nanoparticle in Nitrogen-Rich Carbon Nanotubes as a Bifunctional Electrocatalyst for Hydrogen-Evolution Reaction and Oxygen-Reduction Reaction. *Chem. - Eur. J.* **2017**, *23*, 7710−7718.

(13) Chhetri, M.; Gupta, U.; Yadgarov, L.; Rosentsveig, R.; Tenne, R.; Rao, C. N. R. Effects of p- and n-type Doping in Inorganic Fullerene MoS2 on the Hydrogen Evolution Reaction. *ChemElectroChem* **2016**, *3*, 1937−1943.

(14) Barluenga, J.; Trincado, M.; Rubio, E.; González, J. M. IPy2BF4-Promoted Intramolecular Addition of Masked and Unmasked Anilines to Alkynes: Direct Assembly of 3-Iodoindole Cores. *Angew. Chem. Int. Ed.* **2003**, *42*, 2406−2409.

(15) Wu, J.-X.; He, C.-T.; Li, G.-R.; Zhang, J.-P. An inorganic-MOF-inorganic approach to ultrathin CuO decorated Cu−C hybrid nanorod arrays for an efficient oxygen evolution reaction. *J. Mater. Chem. A* **2018**, *6*, 19176−19181.

(16) Liu, H.; Ma, X.; Rao, Y.; Liu, Y.; Liu, J.; Wang, L.; Wu, M. Heteromorphic NiCo2S4/Ni3S2/Ni Foam as a Self-Standing Electrode for Hydrogen Evolution Reaction in Alkaline Solution. *ACS Appl. Mater. Interfaces* **2018**, *10*, 10890−10897.

(17) Yu, P.-W.; Elmas, S.; Roman, T.; Pan, X.; Yin, Y.; Gibson, C. T.; Andersson, G. G.; Andersson, M. R. Highly active platinum single-atom catalyst grafted onto 3D carbon cloth support for the electrocatalytic hydrogen evolution reaction. *Appl. Surf. Sci.* **2022**, *595*, No. 153480.

(18) Abolghasemi Fakhri, S.; Ashassi-Sorkhabi, H.; Asghari, E.; Taghizadeh, M. T.; Javan, H. Edge-halogenated graphene nanosheets as an efficient metal-free electrocatalyst for hydrogen evolution reaction. *Int. J. Hydrogen Energy* **2022**, *47*, 15731−15741.

(19) Edwards, D. A.; Richards, R.; Myers, R. E.; Walton, R. A. Isoperthiocyanic acid (3-amino-5-thione-l,2,4-dithiazole): an exocyclic sulphur donor ligand. *Inorg. Chim. Acta* **1977**, *23*, 215−219.

(20) Zhang, W.; Chang, J.; Wang, G.; Li, Z.; Wang, M.; Zhu, Y.; Li, B.; Zhou, H.; Wang, G.; Gu, M.; Feng, Z.; Yang, Y. Surface oxygenation induced strong interaction between Pd catalyst and functional support for zinc−air batteries. *Energy Environ. Sci.* **2022**, *15*, 1573−1584.

(21) Kodam, P. M.; Ghadage, P. A.; Nadargi, D. Y.; Shinde, K. P.; Mulla, I. S.; Park, J. S.; Suryavanshi, S. S. Ru, Pd doped WO3 nanomaterials: A synergistic effect of noble metals to enhance the acetone response properties. *Ceram. Int.* **2022**, *48*, 17923−17933.

(22) Liu, X.; Xiang, M.-H.; Zhang, X.; Li, Q.; Liu, X.; Zhang, W.; Qin, X.; Qu, F. An Enzyme-free Electrochemical H2O2 Sensor Based on a Nickel Metal-organic Framework Nanosheet Array. *Electroanalysis* **2022**, *34*, 369−374.

(23) Zhang, W.; Yin, H.; Yu, Z.; Jia, X.; Liang, J.; Li, G.; Li, Y.; Wang, K. Facile Synthesis of 4,4′-biphenyl Dicarboxylic Acid-Based Nickel Metal Organic Frameworks with a Tunable Pore Size towards High-Performance Supercapacitors. *Nanomaterials* **2022**, *12*, No. 2062.

(24) Choi, Y.-H. VO2 as a Highly Efficient Electrocatalyst for the Oxygen Evolution Reaction. *Nanomaterials* **2022**, *12*, 939.

(25) Wang, Z.; Wang, Y.; Zhang, N.; Ma, L.; Sun, J.; Yu, C.; Liu, S.; Jiang, R. Highly efficient oxygen evolution catalysis achieved by NiFe oxyhydroxide clusters anchored on carbon black. *J. Mater. Chem. A* **2022**, *10*, 10342−10349.

(26) Li, W.; Yu, B.; Hu, Y.; Wang, X.; Yang, D.; Chen, Y. Core−Shell Structure of NiSe2 Nanoparticles@Nitrogen-Doped Graphene for Hydrogen Evolution Reaction in Both Acidic and Alkaline Media. *ACS Sustainable Chem. Eng.* **2019**, *7*, 4351−4359.

(27) Gao, W.; Shi, Y.; Zhang, Y.; Zuo, L.; Lu, H.; Huang, Y.; Fan, W.; Liu, T. Molybdenum Carbide Anchored on Graphene Nanoribbons as Highly Efficient All-pH Hydrogen Evolution Reaction Electrocatalyst. *ACS Sustainable Chem. Eng.* **2016**, *4*, 6313−6321.

(28) Yang, L.; Zhang, L.; Xu, G.; Ma, X.; Wang, W.; Song, H.; Jia, D. Metal−Organic-Framework-Derived Hollow CoSx@MoS2 Microcubes as Superior Bifunctional Electrocatalysts for Hydrogen Evolution and Oxygen Evolution Reactions. *J. Mater. Chem. A* **2018**, *6*, 12961−12968.
(29) Thangavel, B.; Berchmans, S.; Venkatachalam, G. Ni@Carbon Nanotubes Derived from Ni-MOF as a Superior Electrocatalyst for Hydrogen Evolution Reaction in Acidic Medium. *Energy Fuels* **2021**, *35*, 1866−1873.
(30) Shu, C.; Du, H.; Pu, W.; Yang, C.; Gong, J. Trace amounts of palladium-doped hollow TiO2 nanosphere as highly efficient electrocatalyst for hydrogen evolution reaction. *Int. J. Hydrogen Energy* **2021**, *46*, 1923−1933.
(31) Sultana, F.; Mushtaq, M.; Wang, J.; Althubeiti, K.; Zaman, A.; Kalsoom Rais, A.; Ali, A.; Yang, Q. An insight to catalytic synergic effect of Pd-MoS2 nanorods for highly efficient hydrogen evolution reaction. *Arabian J. Chem.* **2022**, *15*, No. 103735.
(32) Akbar, K.; Jeon, J. H.; Kim, M.; Jeong, J.; Yi, Y.; Chun, S.-H. Bifunctional Electrodeposited 3D NiCoSe2/Nickle Foam Electrocatalysts for Its Applications in Enhanced Oxygen Evolution Reaction and for Hydrazine Oxidation. *ACS Sustainable Chem. Eng.* **2018**, *6*, 7735−7742.
(33) Wang, Y.; Zhang, Z.; Liu, X.; Ding, F.; Zou, P.; Wang, X.; Zhao, Q.; Rao, H. MOF-Derived NiO/NiCo2O4 and NiO/NiCo2O4-rGO as Highly Efficient and Stable Electrocatalysts for Oxygen Evolution Reaction. *ACS Sustainable Chem. Eng.* **2018**, *6*, 12511−12521.
(34) Kang, Y.; Guo, Y.; Zhao, J.; Jiang, B.; Guo, J.; Tang, Y.; Li, H.; Malgras, V.; Amin, M. A.; Nara, H.; Sugahara, Y.; Yamauchi, Y.; Asahi, T. Soft Template-Based Synthesis of Mesoporous Phosphorus- and Boron-Codoped NiFe-Based Alloys for Efficient Oxygen Evolution Reaction. *Small* **2022**, *18*, No. 2203411.
(35) Solangi, M. Y.; Aftab, U.; Tahira, A.; Abro, M. I.; Mazarro, R.; Morandi, V.; Nafady, A.; Medany, S. S.; Infantes-Molina, A.; Ibupoto, Z. H. An efficient palladium oxide nanoparticles@Co3O4 nanocomposite with low chemisorbed species for enhanced oxygen evolution reaction. *Int. J. Hydrogen Energy* **2022**, *47*, 3834−3845.
(36) Peng, J.; Sun, H.; Ni, K.; Wu, J.; Sun, X.; Su, Y.; Cheng, H.; Liu, Y.; Guo, Y.; Bi, W.; Zhu, Y.; Wu, C.; Xie, Y. Hierarchical Palladium Catalyst for Highly Active and Stable Water Oxidation in Acidic Media. *Natl. Sci. Rev.* **2022**, No. nwac108.
(37) Luo, F.; Zhang, Q.; Yu, X.; Xiao, S.; Ling, Y.; Hu, H.; Guo, L.; Yang, Z.; Huang, L.; Cai, W.; Cheng, H. Palladium Phosphide as a Stable and Efficient Electrocatalyst for Overall Water Splitting. *Angew. Chem., Int. Ed.* **2018**, *57*, 14862−14867.

https://doi.org/10.1021/acsomega.2c04199
ACS Omega 2022, 7, 32604−32614